[UCI]I804:24011-200000237765

2009 年 2 月

碩士學位論文

전기방사를 이용한 나노섬유 제조 및 특성 연구

朝 鮮 大 學 校 大 學 院

化 學 工 學 科

李 允 雅

전기방사를 이용한 나노섬유 제조 및 특성 연구

Fabrication and Characterization of Nanofibers by Electrospinning

2009 年　2 月　　日

朝 鮮 大 學 校 大 學 院

化 學 工 學 科

李　允　雅

전기방사를 이용한 나노섬유 제조 및 특성 연구

指導敎授　金 瑄 日

이 論文을 工學碩士學位 申請 論文으로 提出함.

2008 年　10 月　　日

朝 鮮 大 學 校 大 學 院

化 學 工 學 科

李　允　雅

李允雅의 碩士學位 論文을 認准함

委員長　朝鮮大學校　敎授　車 月 石　印

委　員　朝鮮大學校　敎授　金 瑄 日　印

委　員　朝鮮大學校　敎授　李 在 郁　印

2008 年　11 月　　日

朝 鮮 大 學 校 大 學 院

Acknowledgement

설레임과 기대로 석사 과정을 시작한지 어느덧 2년이라는 시간이 흘러 졸업의 문턱에 서니 감회가 새롭습니다. 지난 시간을 되돌아보면 새로운 환경에서 새로운 것을 배우며 좋은 사람도 많이 만나고 즐거운 일도 많았습니다. 하지만 때로는 여러 가지 상황에 어떻게 대처해야 할지 몰라 고민도 하고 간혹 제가 맡은 일에 실수도 하며 많은 것을 배울 수 있는 시간이었습니다. 석사과정 동안 완성한 논문은 많은 분들의 도움이 있었기에 제게 더욱 깊진 의미가 있으며, 논문의 마지막 페이지를 빌어 도움을 주신 분들께 조금이나마 감사하는 마음을 전하고자 합니다.

먼저 제가 계속 공부를 할 수 있도록 허락해 주시고 언제나 물심양면으로 저에 대한 지원을 아끼지 않으신 부모님과 누나에게 진심으로 감사 드립니다. 젊은 저보다도 세상을 더 도전적으로 살아가시는 부모님 덕분에 항상 많은 것을 배우고 있으며 행복한 가정에서 항상 희망과 용기를 얻을 수 있게 해주심을 또한 감사 드립니다.

석사과정 동안 지도교수님으로서 저의 논문지도 뿐만 아니라 부족한 제게 아낌없는 지원과 가르침으로 많은 도움을 주신 김선일 교수님, 제가 항상 힘을 잃지 않도록 많은 격려를 해주시고 열심히 하는 모습을 보여주셔서 존재만으로도 용기를 북돋아 주셨던 이재욱 교수님 깊이 감사 드립니다. 또한 논문 심사를 위해 시간을 내주시고 많은 조언을 해주신 차월석 교수님, 항상 따뜻한 미소로 격려해주신 조병욱 교수님께도 감사 드리며 학부과정에 들어와서 지금까지 학위과정 동안 많은 가르침을 주신 화학공학과 권규혁, 송연호, 홍완해, 김정규, 이중헌, 신현재 교수님께 진심으로

감사의 마음을 전합니다.

화학공정실험실에서 제가 하는 실험에 많은 조언을 해주시고 올바른 방향으로 갈 수 있도록 세심하게 신경을 써주신 노성희 박사님, 실험과 실험실 생활에 있어서 많은 조언을 해준 경준이형, 항상 열심히 하는 성욱이, 친절한 경량이, 염료감응형 태양전지 테크니션 정성훈, 베트남에서 온 예쁜 Pham Thi Tra 그리고 귀여운 지은이에게 감사의 말씀 전하고 싶습니다. 또한 공학기술연구원에서 격려를 아끼지 않으신 세심한 최도영박사님, 항상 밝은 미소를 잃지 않는 철우형 감사합니다. 석사과정 동안 공대2호관 5층에서 함께 생활해온 승지엄마 손정선 박사님, 폭넓은 지식의 소유자 권세환 사장님, 친절한 환석이 형님, 득여 하신 유성이형, 닌 하우 길록이형, 전장군 경두형, 똑순이 려화누나, 열정의 남규, 완도로 떠난 현우, 실험맨 희준이, 매력남 의진이, 중국에서 유학 온 춘화, 형님 은선이, 작년에 졸업한 홍일이형, 고운이, BK21 최수경 박사님과 남숙이, 그리고 학부생 유란이, 보미에게 고마움을 전합니다. 그리고 기쁠때나 힘들때나 항상 함께한 친구 안진, 덕현, 도정, 경빈이 그리고 든든한 후배 태양이, 세훈이, 명진이, 광수, 병철이와 이 기쁨을 함께하고 싶습니다.

앞으로도 많이 경험하고 많이 배우는 길을 가고 싶습니다. 새로운 것을 시작한다는 것은 항상 저를 설레이게 합니다. 소중한 추억과 지난 과정들은 분명 좋은 결과의 밑거름이 될 것이라고 믿습니다.

2008年 12月 16日

이윤아 올림

Contents

LIST OF TABLES

LIST OF FIGURES

ABSTRACT

전기방사를 이용한 나노섬유 제조 및 특성 연구

Yoon-Ah Lee

Advisor : Prof. Sun-Il Kim, PhD.

Department of Chemical Engineering

Graduate School of Chosun University

전기방사(Electrospinning) 기술은 고분자, 세라믹, 금속 및 복합체 등 다양한 소재들의 나노섬유를 제조할 수 있는 매우 유용한 기술이다. 부피 대비 높은 비표면적을 지닌 나노섬유들은 저렴하고 간단한 공정으로 제조할 수 있는 이 기술을 활용하여 생명과학, 의료, 군사, 환경, 에너지 및 전자소재 및 소자 등 다양한 분야에서 응용연구가 진행되고 있다. 본 연구에서는 전기방사를 이용하여 탄소 나노섬유, 실리카 나노섬유 그리고 TiO_2 나노섬유를 제조하여 그 특성을 SEM, TGA, XRD, FT-IR 그리고 BET 기기분석을 하였다. 첫째, 온도에 따른 탄소나노섬유를 제조하여 KOH를 첨가하여 열처리 후에 얻은 탄소물질을 이용하여 환경을 오염시키는 Congo Red 와 Bisphenol-A 를 제거하는 흡착 평형 실험을 수행하였다. 그 결과 시중에서 판매하고 있는 활성탄 보다 표면적 및 흡착량이 더 우수함을 확인할 수 있었다. 둘째, 고분자공중합체인 pluronics P123 를 지지체로 하여 전구물질인 tetraethyl orthosilicate (TEOS) 를 이용하여 200 ~ 300 nm 의 직경을 가진 실리카 나노섬유를 제조하였다. 제조된 실리카 나노섬유를 이용하여 단백질인 lysozyme 흡착 평형 실험을

실시하여 Langmuir 흡착등온선에 적합함을 알 수 있었다. 마지막으로 titanium(IV)-isopropoxide 전구물질을 이용하여 섬유 직경이 80~100 nm 인 TiO_2 나노섬유를 제조하여 특성을 조사하고 표면을 $TiCl_4$ 용액으로 처리하여 염료감응형 태양전지(dye-sensitized solar cell)에 적용하여 10% 효율 향상을 얻을 수 있었다. 전기방사를 이용한 나노섬유 제조는 다양한 종류의 고분자와 용매를 조합하고, 공정 변수들을 조절함으로써 다양한 기능성 나노섬유의 재조가 가능하기 때문에 일반 소재, 전자 소재, 의료 소재 분야 등 그 용도는 대단히 폭 넓을 것으로 사료된다.

Chapter 1. Introduction

1.1. History of Electrospinning

Electrospinning traces its roots back to electrostatic spray painting, which has been in operation for almost 100 years. In 1934, a process for the production of polymer filaments using electrostatic force was patented by Formhals.[1] Formhals encountered a number of problems early in his work, but by 1940 he had not only overcome those initial problems, he had developed methods of producing composite fibers using multiple polymers and for producing fibers that were aligned parallel to one another. Although the fibers produced by Formhals were much larger than the nanofibers that will be of concern in this paper, his work set the stage for the production of these structures.

Taylor[2] did a study of the polymer droplet at the end of the needle in an electrospinning setup in 1969. This study led to a better understanding of the process by which the polymer solution streams from the needle. In 1987, the experimental conditions and factors that cause highly conductive fluids exposed to increasing voltages to produce unstable streams was studied by Hayati et al.[3] These conditions cause the fluid stream to whip around in different directions as it leaves the needle. The work of Doshi and Reneker[3] explored how changing the concentration of the polymer solution and the voltage applied to the solution affected the formation of nanofibers.

Numerous other studies have been done to examine the effect of changing both the polymer solution and the experimental setup. Based on these studies it is clear that characteristics such as fiber diameter, fiber morphology and the amount of beading are dependent upon a large number of variables. These variables include solution concentration, viscosity, surface tension and conductivity and process variables, such as voltage, needle diameter, flow rate and needle-to-

collector distance.

1.2. Fundamentals of Electrospinning

The formation of nanofibres through electrospinning is based on the uniaxial stretching of a viscoelastic solution. To understand and appreciate the process that enables the formation of various nanofibre assemblies, the principles of electrospinning and the different parameters that affect the process have to be considered. Unlike conventional fibre spinning methods like dry-spinning and melt-spinning, electrospinning makes use of electrostatic forces to stretch the solution as it solidifies. Similar to conventional fibre spinning methods, the drawing of the solution to form the fibre will continue as long as there is enough solution to feed the electrospinning jet. Thus without any disruption to the electrospinning jet the formation of the fiber will be continuous.

Fibers with a diameter of between 100 nm-500 nm are generally classified as nanofibers (Figure 1). These fibers can be made from a wide variety of materials ranging from metals to ceramics to polymers. What makes nanofibers of great interest is there extremely small size. With higher surface area to volume ratios and smaller spaces between individual fibers than larger fibers, nanofibers offer an opportunity for use in a wide variety of applications. Increased awareness of the current and the potential applications of nanofibers have in recent years accelerated the research and development of these structures.

Some important applications for these nanofibers include, but are not limited to, catalytic substrates, photonics, filtration, protective clothing, cell scaffolding, drug delivery and wound healing. Different applications may require the fibers to possess different properties. For instance, one application might require the nanofibers to be hydrophobic or hydrophilic; another may need the fiber to be biodegradable or biocompatible. It will, therefore, be extremely important to

completely understand the process by which these fibers are produced. To date, the most successful method of producing nanofibers is through the process of electrospinning.

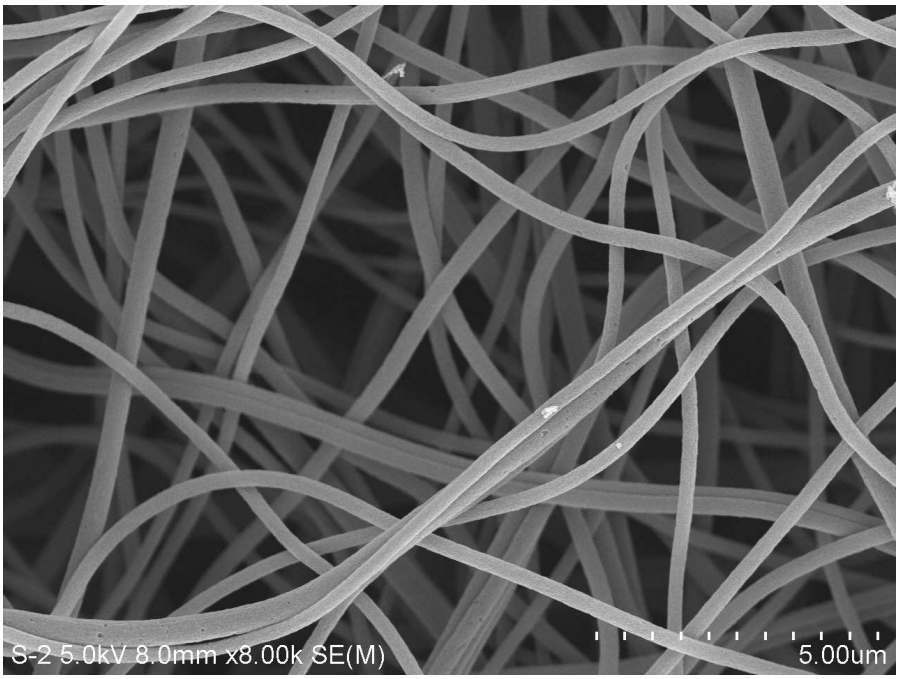

Figure 1. Nanofibers by electrospinning.

The electrospinning process uses high voltage to create an electric field between a droplet of polymer solution at the tip of a needle and a collector plate (Figure 2). One electrode of the voltage source is placed into the solution and the other is connected to the collector. This creates an electrostatic force. As the voltage is increased, the electric field intensifies causing a force to build up on the pendant drop of polymer solution at the tip of the needle. This force acts in a direction opposing the surface tension of the drop. The increasing electrostatic force causes the drop to elongate forming a conical shape known as a Taylor cone[2] (Figure 3). When the electrostatic force overcomes the surface tension of the drop, a charged, continuous jet of solution is ejected from the cone. The jet of solution accelerates towards the collector, whipping and bending wildly.

As the solution moves away from the needle and toward the collector, the jet rapidly thins and dries as the solvent evaporates. On the surface of the grounded collector, a nonwoven mat of randomly oriented solid nanofibers is deposited.

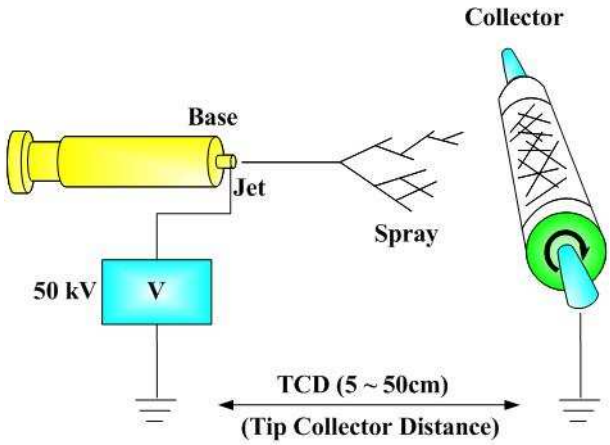

Figure 2. Electrospinning apparatus.

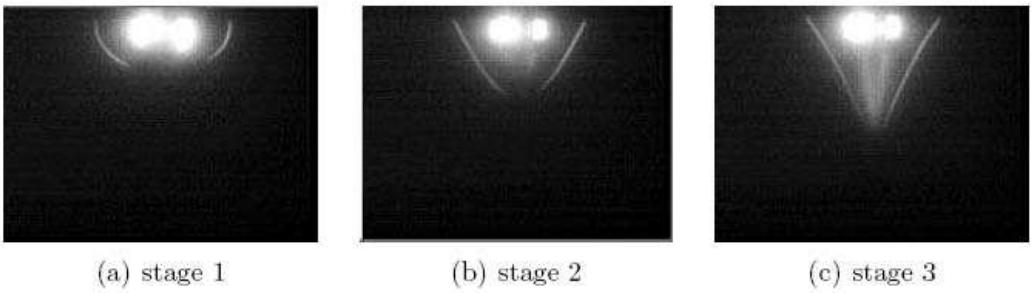

Figure 3. Formation of the Taylor cone. Voltage increases with each stage until equilibrium between surface tension and the electrostatic force is achieved in stage 3.

1.3. Objectives

Chapter 2 deals with adsorption of carbon nanofibers synthesized by electrospinning polyacrylonitrile solution. This study focuses on the adsorption properties of carbon nanofibers(CNFs) fabricated by electrospinning polyacrylonitrile solutions dissolved in dimethylformamide, followed by heat treatment at high temperatures (400, 600, 800 and 1000℃). The samples were characterized by SEM, TGA and BET. In addition, the adsorption energy distribution functions of CNFs were analyzed by using the generalized nonlinear regularization method. Comparative analysis of energy distribution functions provided significant information on the energetic and structural heterogeneities of CNFs. Furthermore, an investigation of adsorption equilibrium of congo red(CR) and bisphenol-A(BPA) revealed the adsorption capacity. Our experimental and theoretical results suggest that the CNFs used in this work may be widely used as an adsorbent.

Chapter 3 describes preparation and characterization of electrospun silica nanofibers from PVP/P123 blended polymer solution. Silica nanofibers were prepared by electrospinning method using PVP/P123 blend polymer solutions. Here, a triblock copolymer (Pluronic P123, $EO_{20}PO_{70}EO_{20}$, M_{av}=5800) was used as the structure directing agent and polyvinyl pyrrolidone (PVP) as the fiber template. The samples were characterized by scanning electron microscopy (SEM), Fourier Transform Infrared (FT-IR), X-ray diffraction (XRD), TGA (thermal gravimetric analysis), and Brunauer-Emmett-Teller (BET). It was found that the silica nanofibers synthesized in this work had uniform pore structure with high surface area. An average fiber diameter, average pore diameter, and surface area were about 300 nm, 2.7 nm and 607 $m^2 g^{-1}$. Adsorption equilibrium data of lysozyme on the synthesized silica nanofibers were correlated well with Langmuir equation.

Chapter 4 investigates preparation and characterization of electrospun TiO_2 for dye-sensitized solar cell. It has been known that electrspun TiO_2 nanofibers can be applied for an electrode for dye-sensitized solar cells (DSSC). Therefore, this paper reports on structural characterization and morphology of titanium dioxide (TiO_2) nanofibers prepared by electrospinning using a solution that contained polyvinyl acetate (PVA) and titanium(IV) isopropoxide and acetic acid as a catalyst for sol-gel reaction in dimethyl formamide. TiO_2 nanofibers with diameters of 80-100 nm were successfully obtained from calcination of the as-electrospun TiO_2/PVA composite nanofibers at above 400℃ in air for 5h. The samples of as-electrospun and calcined TiO_2/PVA composite nanofibers were characterized by SEM, XRD, FT-IR, TGA, and BET. The results indicated a significant effect of calcination temperature on the crystalline phase in the form of either anatase or mixed anatase-rutile as well as the morphology of the nanofibers.

Chapter 2. Adsorption of Carbon Nanofibers Synthesized by Electrospinning Polyacrylonitrile Solution

2.1. Introduction

Carbon fibers have been prepared from a wide variety of precursors in the range from natural materials to various thermoplastic and thermosetting precursor materials. Among them, polyacrylonitrile (PAN) is one of the most widely used precursor in carbon fiber industry. The carbon yield strongly depends on the chemical and morphological structures of the precursor fibers. In general, PAN-based carbon fibers have lower carbonization yield than aromatic structure based precursors, such as pitch, phenol, polybenzimidal, polyimide etc.

Electrospinning has shown to be a simple but powerful technique for the preparation of fibers with submicrometer diameters [4-6]. In the recent years, the electrospun fibers have attracted lots of attentions due to their wide range of potential applications such as tissue engineering, sensor, protective clothing, high performance filter, functional nano carbon materials etc. In this chapter, CNF was fabricated by electrospinning the PAN dissolved in dimethylformamide. The samples were characterized by SEM, TGA and BET. In addition, the surface heterogeneity of CNF was evaluated on the basis of the adsorption energy distribution functions calculated by a generalized nonlinear regularization method. To understand the adsorption properties of CNF, the adsorption equilibrium of congo red(CR) and bisphenol-A(BPA) were studied. Adsorption isotherm was evaluated by a simple adsorption model which was formulated by incorporating the Langmuir, Freundlich and Sips isotherm.

2.2. Experimental

2.2.1. Preparation of carbon nanofibers

Precursor (polyacrylonitrile (PAN), molecular weight = 160,000) and solvent N,N-dimethylformamide (DMF) (99.9%)) were obtained from Aldrich Chemical Co (USA). PAN (10 wt%) with regard to solvent were dissolved in DMF at 60℃ to obtain polymer solution. The solution was spun into fiber web through a positively charged capillary using an electrospinning apparatus at 20 kV. The negative electrode was connected to a drum winder collecting the fiber web. The electrospun fibers were collected as web on an aluminum foil wrapped on the metal drum with a rotation speed ~ 300 rpm. The electrospun fiber web was stabilized in an air atmosphere at 280℃ for 1hr (heating rate: 1℃/min), then carbonized in an inert atmosphere up to 400, 600, 800, 1000℃(heating rate: 5℃/min). The soaking time at 400, 600, 800, 1000℃ was 1hr in an electrical furnace under N_2 gas. Carbon fibers were mixed and KOH (sample : KOH =1:4) was added, then heated in an inert atmosphere up to 800℃(heating rate: 5℃/min) during 1hr under N_2 gas.

2.2.2. Characterization

The nanofiber surface was analyzed by using a scanning electron microscope (SEM Hitachi, S-4700, Japan). Thermal gravimetric analysis (TGA) was employed to evaluate the weight loss of the samples in air under a heating rate of 10 ^{o}C/min using a thermal analyzer (Perkin-Elmer PYRIS 1). Nitrogen physisorption isotherms were measured on a micromeritics ASAP 2010 analyzer at 77K. The specific surface areas were evaluated using the Brunauer-Emmett-Teller (BET) method. The pore size distribution was calculated using the Barrett-Joyner-Halenda (BJH) method based on the adsorption branch of the isotherms, and the average pore size was reported from the peak

position of the distribution curve. The pore volume was taken at the $P/P_o = 1.00$.

2.2.3. Adsorption of Congo red and Bisphenol-A

The adsorption experiments were carried out using two commercially available adsorbate, namely, Congo Red(CR) and Bisphenol-A(BPA), purchased from Aldrich Co. (USA). Their chemical structures and properties are listed in Table 1. The adsorption experiments were conducted by adding different amounts of CNF into a flask containing 100 ml of CR and BPA solutions. After shaking in a constant temperature incubator at constant temperature (298.15 K) for 3 days to give sufficient contacting time for equilibrium, samples were taken from the flask and filtered through a 0.2 ㎛ HT Tuffryn membrane filter. The adsorption capacity (q) of carbon fibers was determined from the expression

$$q = \frac{V(C_o - C)}{m} \tag{1}$$

Where, C_o and C are the initial and equilibrium (or residual) liquid-phase concentrations (mg L^{-1}), respectively, V is the volume of solution (L), and m is the weight of dry activated carbon (g). The amount of CR and BPA adsorbed on adsorbent was calculated by the mass balance before and after adsorption.

The filtrate was then measured for the CR and BPA concentration. The CR and BPA concentration was evaluated using a UV spectrophotometer (UV-1700 Shimadzu) at 497 nm and 275 nm for CR and BPA, respectively. Solution pH was determined by using the pH meter(Orion, USA).

Table 1. Properties of Asorbates

Adsorbates (molecular weight)	Structure	λ_{max} (nm)	Solubility, mg l^{-1} at 20℃
Bisphenol-A (228 g mol^{-1})	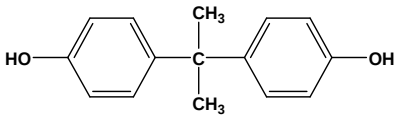	276	120 ~ 130
Congo Red (697 g mol^{-1})	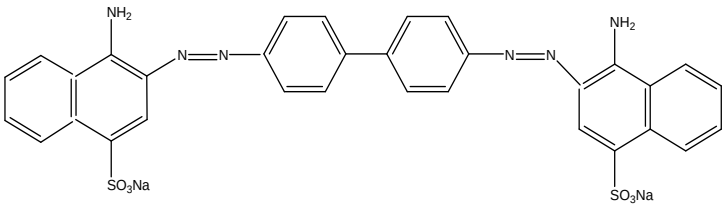	497	40,000

2.3. Results and Discussion

The fiber surface area and the diameter were analyzed by using a scanning electron microscope (SEM). Figure 4 shows an example of scanning electron micrographs for CNFs showing a highly uniform diameter distribution.

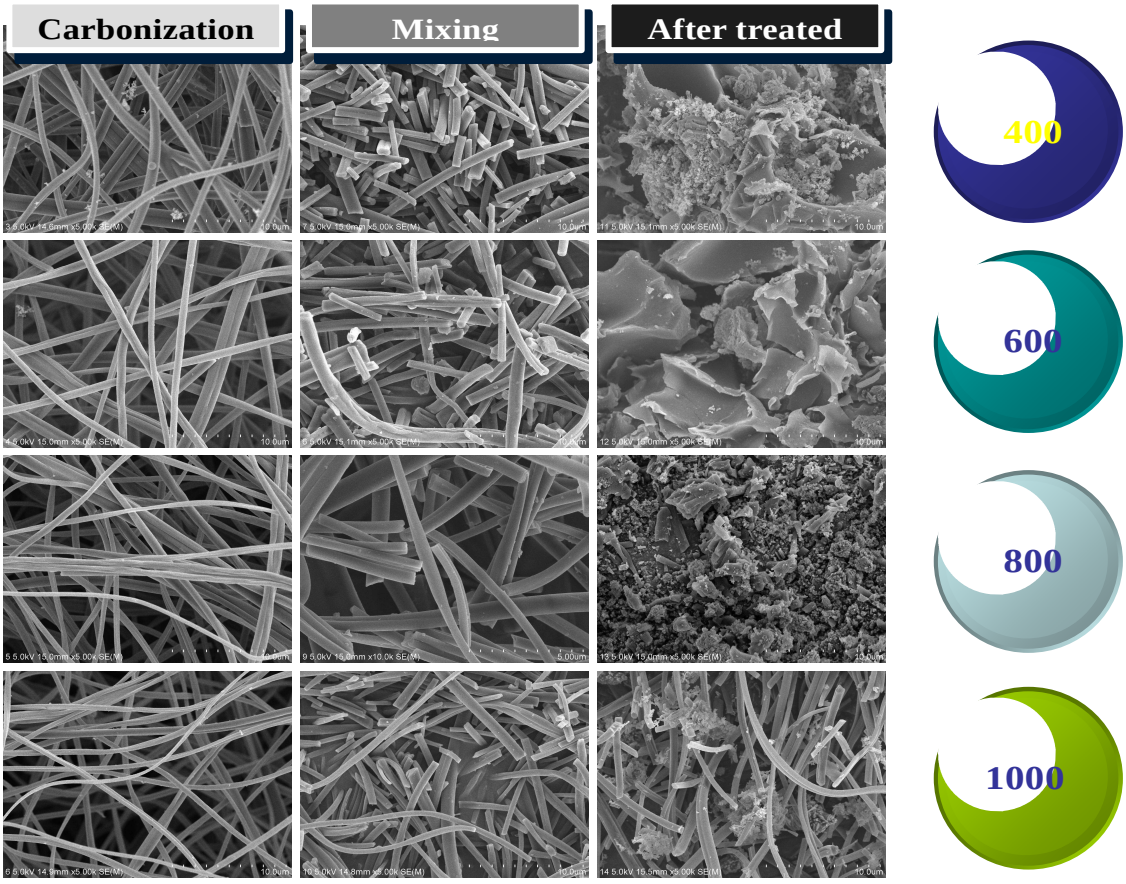

Figure 4. SEM images of carbon nanofibers.

The TGA curve of the as-electrospun PAN fibers showed two steps and a total loss of ca. 80% (Figure 5). The 20% of weight loss occurred at around 280℃, which eliminate water, and induces the aromatization of carbon.

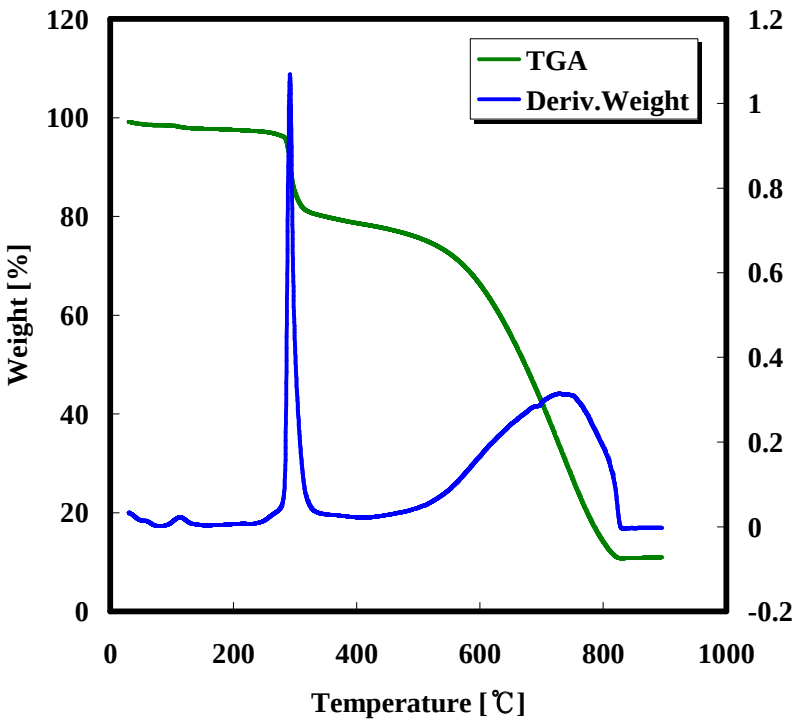

Figure 5. TGA curve of PAN nanofibers.

Nitrogen adsorption-desorption isotherms were measured on an ASAP 2010 volumetric adsorption apparatus (Micrometrics) at 77.4 K (Fig. 6). The surface area was calculated by the BET method. The pore size distribution was obtained by density functional theory (Figure 6). The surface area was found to be in the range of 1382.03 ~ 1428.23 m^2 g^{-1} and the average pore diameter 28 Å. The physical properties determined are listed in Table 2.

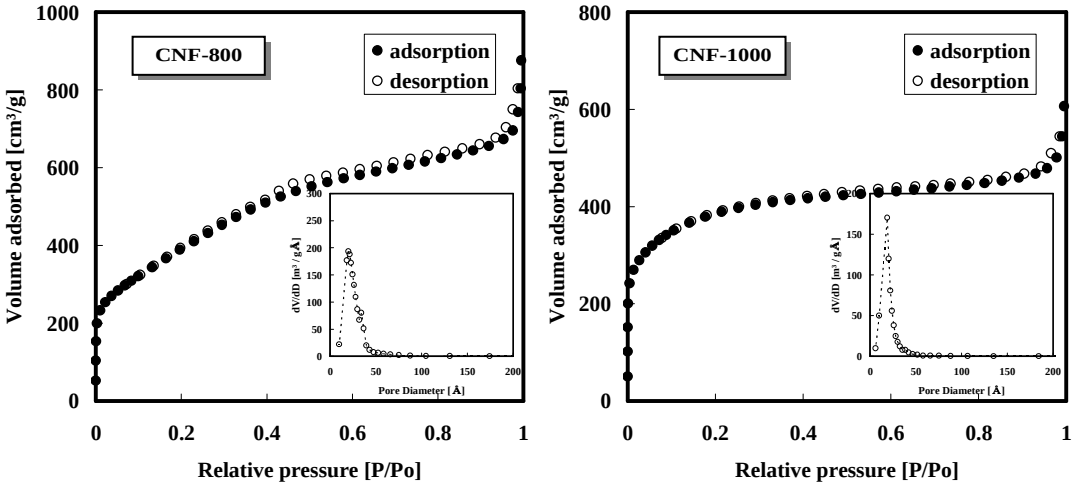

Figure 6. Nitrogen adsorption-desorption isotherms of carbon nanofibers

Table 2. Characteristics of Adsorbents

Specification	CNF-800	CNF-1000	PAC – CB
Raw material	Carbon fiber	Carbon fiber	Coal - based
BET surface area [$m^2 g^{-1}$]	1,428	1,382	915
Total pore volume [$cm^3 g^{-1}$]	1.21	0.47	-
Average pore width [Å]	28.6	28.0	24.2

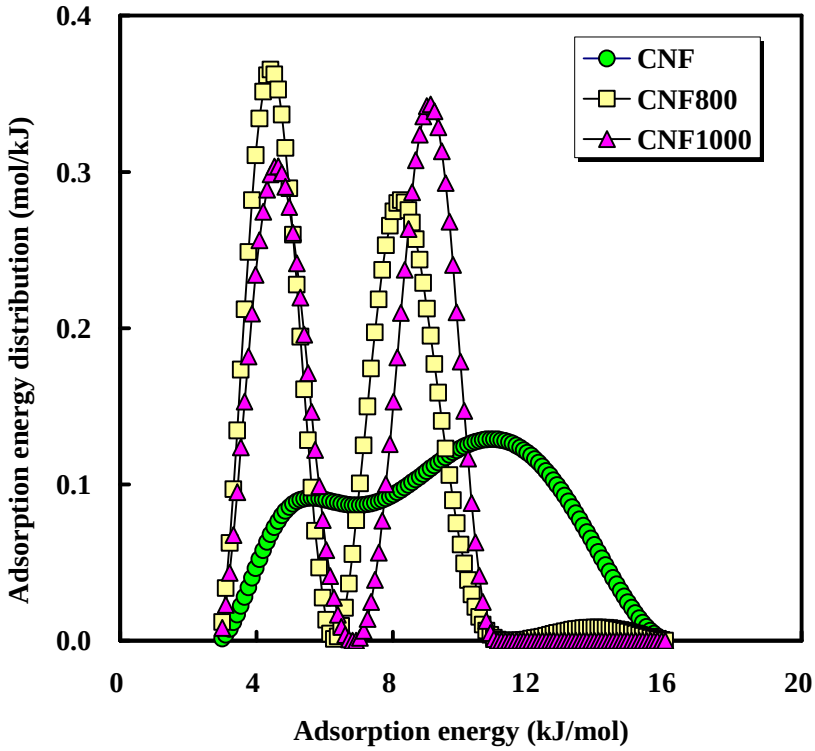

Figure 7. Adsorption energy distribution curves of CNFs.
(CNF is untreated, CNF-800 and CNF-1000 are treated with KOH)

Adsorption energy distributions have been extensively applied in characterizing the numerous adsorption systems and in understanding the physico-chemical networks related to surface energy heterogeneities. Experimental adsorption isotherm data have been crucial factors for characterizing the surface energy heterogeneity of adsorbent.[7] Also, a theoretical local adsorption isotherm equation and an adsorption energy distribution function should be included. The overall adsorption isotherm on the heterogeneous solid surface can be written in the form of

$$\theta_T(p) = \int_\Delta \theta_L(p,U) \cdot F(U) dU \tag{2}$$

where p is the equilibrium pressure, Δ is the integration region, $\boldsymbol{U}$ is the adsorption energy, $\boldsymbol{F(U)}$ is the wanted energy distribution function, $\theta_L(p,U)$ is a local adsorption isotherm and $\theta_T(p)$ is the experimental adsorption isotherm data. In this work, we employed the generalized regularization method to obtain reliable and stable adsorption energy distributions.[8] The adsorption energy distributions of CNFs (CNF-800, CNF-1000) activated at different temperatures are presented in Figure 7. The highest adsorption energy peaks for CNF-800 was found to be around 6, 10 kJ mol^{-1}. Unlike CNF-800 and CNF-1000 with a relative large surface area has two main adsorption energy peaks with lower energy intensity. It was found from the result of adsorption energy distribution that CNFs used in this work are energetically and structurally heterogeneous surfaces.

Adsorption isotherms are the most important information for analyzing and designing an adsorption process.[9] Figure 8,9 shows the adsorption isotherms of CR and BPA on CNFs at 298.15 K. The adsorption capacity depends on the properties of the adsorbate and the adsorbent. The adsorption capacity of BPA was much higher than that of CR. In addition, the adsorption capacity of CR and BPA on CNFs was ordered as CNF-800 > CNF-1000 since the specific surface area increased with increasing activation temperature.

Table 3. Adsorption Isotherm Equations

Isotherm Type	Equation	Parameters
Langmuir	$q = \frac{q_m bC}{1+bC}$	q_m, b
Freundlich	$q = kC^{1/n}$	k, n
Sips	$q = \frac{q_m bC^{1/n}}{1+bC^{1/n}}$	q_m, b, n

Among the well-known isotherms such as the Langmuir, Freundich and Sips isotherm models (Table 3), the adsorption equilibrium data of Congo red on PAC, CNF-800 and CNF-1000 were correlated by the Freundlich equation. On the other hand, the adsorption equilibrium data of Bisphenol-A on PAC, CNF-800 and CNF-1000 were correlated by the Sips equation.

The isotherm parameters were determined by minimizing the mean percentage deviations between experimental and predicted amounts adsorbed, based on a modified Levenberg-Marquardt method (IMSL routine DUNSLF). The object function, E (%), represents the average percent deviation between experimental and predicted results as follows:

$$E(\%) = \frac{100}{n}\sum_{k=1}^{n}\left[\frac{\left|q_{\exp,k} - q_{cal,k}\right|}{q_{\exp,k}}\right] \tag{3}$$

Here, n is the number of experimental data, $q_{exp,k}$ is the experimental adsorption capacity, and $q_{cal,k}$ the calculated adsorption capacity. The solid lines (Figure 8) are the predicted results with Freundlich isotherm parameters (Table 4) of CR on PAC, CNF-800 and CNF-1000. Figure 9 are the predicted results with Sips isotherm parameters (Table 5) of BPA on PAC, CNF-800 and CNF-1000. Judging from the experimental and theoretical results obtained in this work, it seems that PAN-based CNFs by electrospinning can be used as an adsorbent.

Table 4. Isotherm Parameters for Congo Red at 298.15 K and pH 7

Adsorbent	Isotherms	Parameters		E(%)
PAC-CB	Langmuir	q_m	73.53	4.51
		b	2.31	
	Freundlich	k	53.94	0.72
		n	10.27	
	Sips	q_m	101.15	1.36
		b	1.09	
		n	3.54	
CNF-800	Langmuir	q_m	161.29	14.78
		b	8.86	
	Freundlich	k	112.35	2.77
		n	6.24	
	Sips	q_m	265.43	5.59
		b	0.77	
		n	2.91	
CNF-1000	Langmuir	q_m	158.73	11.24
		b	12.6	
	Freundlich	k	119.62	2.43
		n	8.57	
	Sips	q_m	229.93	3.90
		b	1.18	
		n	3.33	

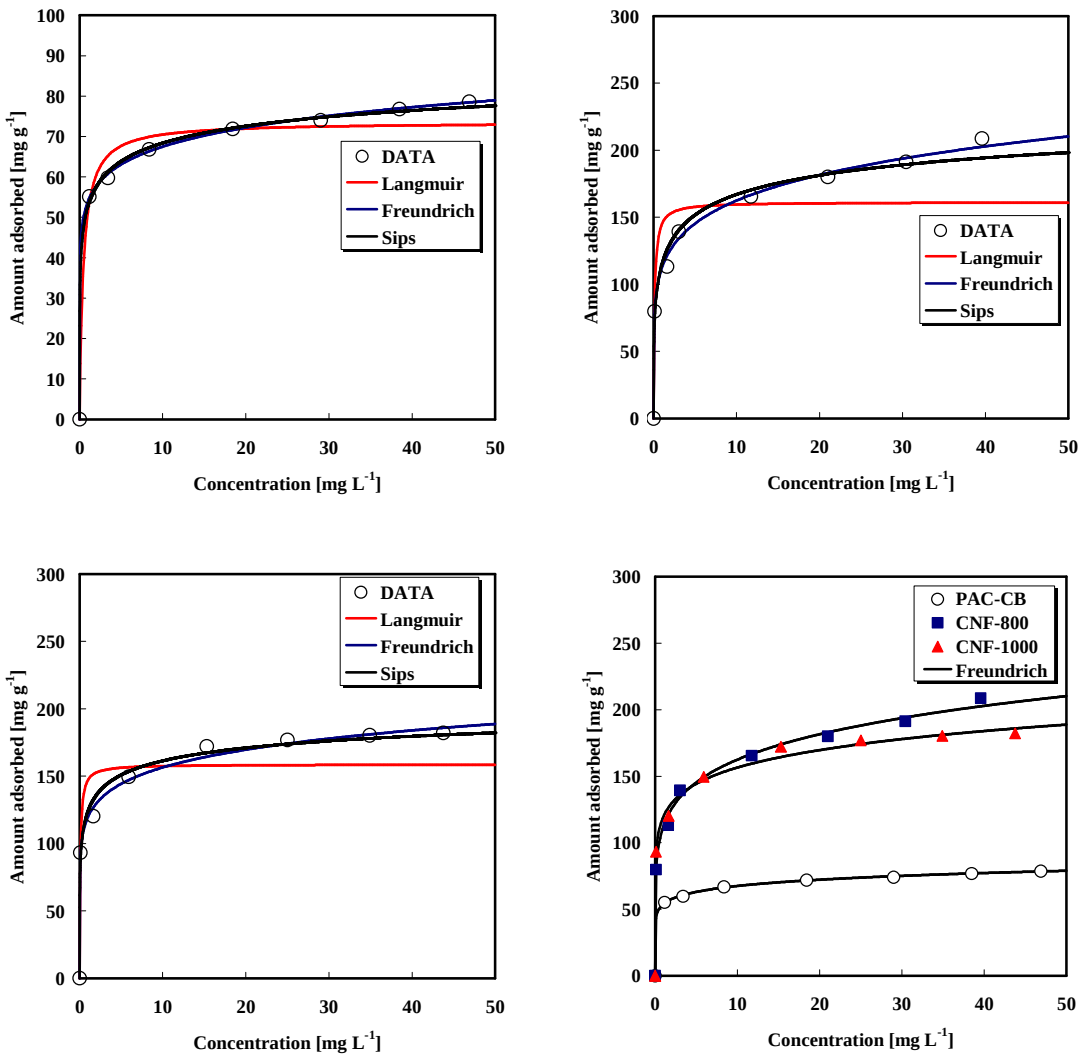

Figure 8. Adsorption isotherm of congo red on PAC-CB(a), CNF-800(b) and CNF-1000(c) at pH 7 and 298.15 K.

Table 5. Isotherm Parameters for Bisphenol-A at 298.15 K and pH 7

Adsorbent	Isotherms	Parameters		E(%)
PAC-CB	Langmuir	q_m	238.10	4.11
		b	1.40	
	Freundlich	k	154.70	1.49
		n	8.81	
	Sips	q_m	280.73	1.11
		b	1.08	
		n	2.25	
CNF-800	Langmuir	q_m	294.12	5.19
		b	0.74	
	Freundlich	k	148.65	3.37
		n	5.67	
	Sips	q_m	335.41	2.30
		b	0.63	
		n	1.59	
CNF-1000	Langmuir	q_m	277.78	4.25
		b	1.71	
	Freundlich	k	168.36	3.54
		n	7.64	
	Sips	q_m	325.60	1.72
		b	1.05	
		n	2.20	

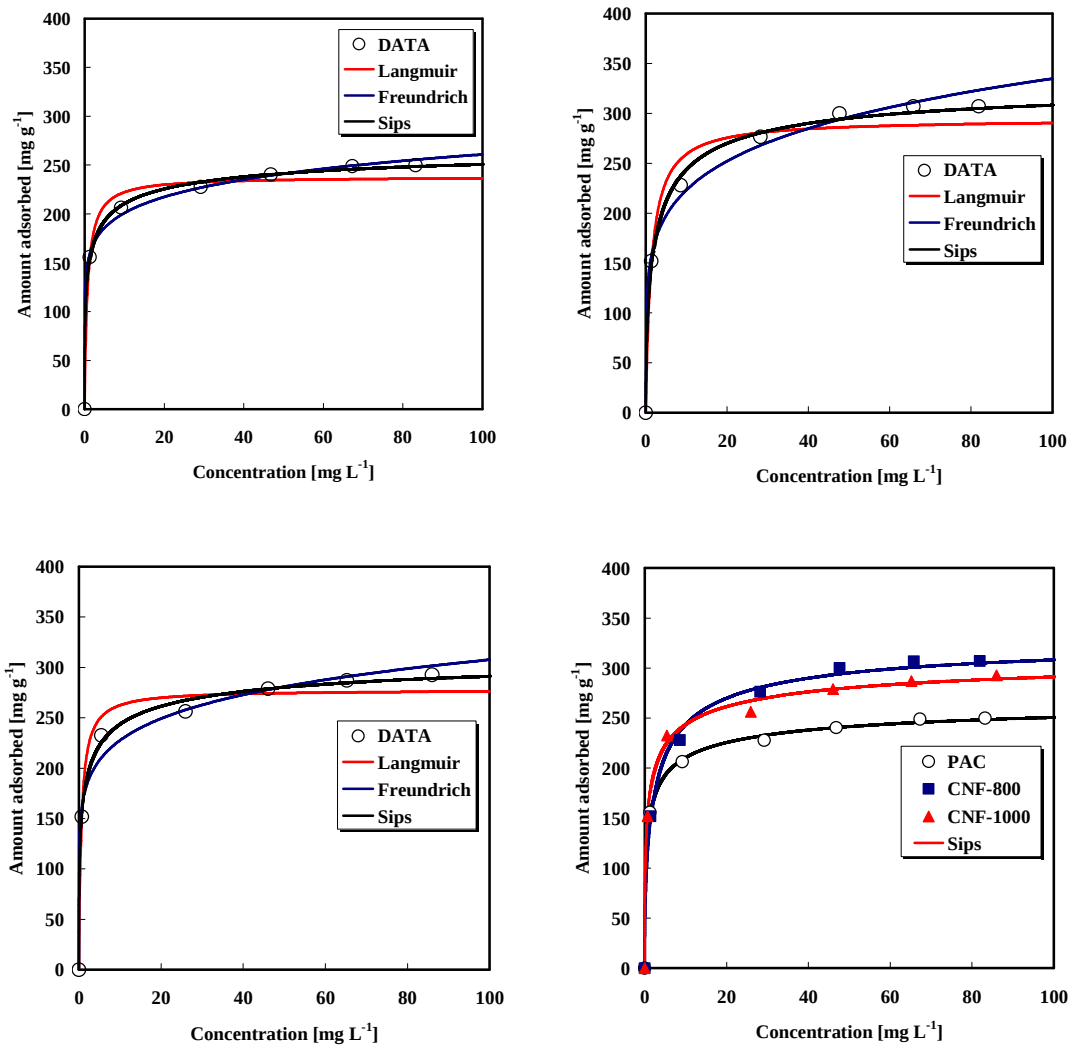

Figure 9. Adsorption isotherm of Bisphenol-A on PAC-CB(a), CNF-800(b) and CNF-1000(c) at pH 7 and 298.15 K.

2.4. Conclusion

For the application of CNF fabricated by electrospinning of polyacrylonitrile solutions, adsorption equilibrium were investigated. Adsorption equilibrium data of CR and BPA were correlated well with Freundlich and Sips equation respectively. We found that the adsorption capacity of CR and BPA was CNF-800 > CNF-1000. The result of adsorption energy distribution revealed that the CNFs used are energetically and structurally heterogeneous surfaces. The adsorption equilibrium study indicates that carbon nanofibers can successfully be applied for many adsorption fields.

Chapter 3. Preparation and Characterization of Electrospun Silica Nanofibers from PVP/P123 Blended Polymer Solution

3.1. Introduction

A advanced class of materials, mesoporous silicates and aluminosilicates denoted as M41S (i.e., MCM-41, MCM-48, MCM-50 and other species) have been the subject of much interest since they were first described by the Mobil Oil scientists in 1992.[9] These potential materials have been explored for promising applications in the field of sensor, chromatographic packing material, catalytic support, immobilized medium, template of advanced nano-materials, adsorption, and catalytsis.[10-16] The synthesis and utilization of these materials have been investigated by many researchers because of their unique characteristics such as large internal surface area, uniformity of pore size, easily controlled pore size, and high thermal stability. Many researchers have focused on the fabrication of ordered mesoporous materials and obtaining in the improved catalytic activities.[17] Besides these results, many attempts have been made to investigate the benefits of silica nanofibers in the areas of sensors, catalysts, separations and drug delivery. It has been known that electrospinning is a relatively simple and efficient method to produce fibers with diameters in the nanometer to micro range from the precursor gels.[18,19] Unfortunately, the synthesis of nanofibers from the blend solutions consisting of polymer and inorganic materials have very limited data.

Here in present study, we report the preparation of silica nanofibers by electrospinning PVP/P123 blend polymer solutions. For this, a triblock copolymer (Pluronic P123, $EO_{20}PO_{70}EO_{20}$, M_{av}=5800) and polyvinyl pyrrolidone (PVP) were used as the structure directing agent and the fiber

template, respectively. The synthesized nanofibers were characterized by Fourier Transform Infrared (FT-IR), X-ray diffraction (XRD), TGA (thermal gravimetric analysis), and Brunauer-Emmett-Teller (BET). Also, adsorption properties of lysozyme were examined to evaluate the synthesized silica nanofiber as an adsorbent.

3.2. Experimental

3.2.1. Preparation of Silica Nanofibers

The chemicals used in this study include tri-block copolymer poly(ethylene oxide)-poly(propylene oxide)-poly(ethylene oxide), pluronics P123 (MW: 5800, Aldrich), tetraethyl orthosilicate (TEOS, 98%, Aldrich), and PVP (MW: 1.3×10^6, Aldrich). Analytical pure hydrochloric acid and ethanol were obtained from Duksan (Korea). The precursor solution was prepared from PVP ethanol solution using P123 as structure directing agent. TEOS (3 g), P123 (1 g), and PVP (2.3 g) were dissolved in ethanol (20 g) using magnetical stirrer at room temperature for 1 h to obtain homogenous solution. HCl (0.2 g, 2 M) was added drop wise to the solution for the hydrolyzation of TEOS. Then the solution was refluxed at 70–80 °C and kept stirred for 1 h.

Figure 2 shows the experimental apparatus of electrospinning. The precursor solutions were taken into a 5 ml syringe with a capillary tip having an inner diameter of 0.6 mm. A wire inserted into the solution was connected to a high-voltage power supply. The applied voltage was fixed at 20 kV and a tip-to-collector distance was 20 cm. Aluminum foil was used as a collector attached to the cathode. The as-electrospun silica/PVP fibers were calcined in a muffle furnace which was heated from room temperature to 550 °C in air under a rate of 5 °C /min. The produced fibers were stabilized at 550 °C for another 2 h. The silica nanofibers were finally obtained after the temperature decreased to room temperature.

3.2.2. Characterization

Scanning electron microscopy (SEM) was carried out on a Hitachi S-4800 electron microscope. Fourier Transform Infrared (FT-IR) spectra were observed by using FT-IR-410 Jasco. X-ray diffraction (XRD) patterns were obtained on a PANalytical (Philips) X'Pert PRO MRD diffractometer using Cu Kα radiation source of wavelength 1.5406 Å for 2theta ranging from 0.01^o to 5° with a scan speed of 3.0^o/min at 40kV and 30 mA. Thermal gravimetric analysis (TGA) was employed to evaluate the weight loss of the samples in air under a heating rate of 10 ℃/min using a thermal analyzer (Perkin-Elmer PYRIS 1). Nitrogen physisorption isotherms were measured on a micromeritics ASAP 2010 analyzer at 77K. The specific surface areas were evaluated using the Brunauer-Emmett-Teller (BET) method. The pore size distribution was calculated using the Barrett-Joyner-Halenda (BJH) method based on the adsorption branch of the isotherms, and the average pore size was reported from the peak position of the distribution curve. The pore volume was taken at the $P/P_o = 1.00$.

3.2.3. Protein Adsorption

Batch adsorption experiments were carried out by contacting 50 mg of the silica nanofibers with 10 mL of different protein concentrations in buffer solution. In order to prevent microbial contamination, sodium azide was added into the solution. The adsorbent and solution were sealed and kept in a shaking incubator with a speed of 300 rpm for 12 h. The supernatant liquid was diluted in a buffer solution and then filtered through a 0.2 ㎛ HT Tuffryn low protein binding membrane filter. The protein concentration in the supernatant was analyzed with a UV spectrophotometer (UV-1700 Shimadzu) at 280 nm. The amount of protein adsorbed on adsorbent was calculated by the mass balance before and after adsorption.

3.3. Results and Discussion

The morphologies of electrospun silica/PVP fibers and the silica nanofiber were uniform in size and had smooth surfaces (Figure 10). The average diameter of the fibers was evaluated by choosing 100 fibers among x1000 magnification SEM images and analyzing them using a custom code image-analysis program. The average diameter of the as-electrospun silica/PVP fibers and silica nanofibers were in the range of 500-700 nm and 200-400 nm. FT-IR experiment was employed to prove the removal of the surfactant and polymer (Figure 11(a1)~(a3)). Absorption at 2970, 2922 and 1464 cm^{-1} (Figure 11(a1)) is attributed to CH_2 absorption of P123 surfactants and PVP. Also, absorption at 1290 cm^{-1} (Figure 11(a1)) and 1292 cm^{-1} (Figure 11(a2)) were consistent with the absorption of tertiary amine group of PVP. However these bands were not observed in the silica nanofiber. The result implies that the thermal treatment was reasonably effective at removing P123 and PVP. The evident absorption at 1092, 804, and 466 cm^{-1} (Figure 11(a3)) showed the existence of the silica structure corresponding to the Si–O–Si flexural vibrations. XRD pattern of the silica nanofibers indicated that the samples showed that one strong peak was observed at the $2\theta=0.97°$ corresponding (100) reflection of SBA-15 (Figure 11(b)). The TGA curve of the as-electrospun silica/PVP fibers showed two steps and a total loss of ca. 70% (Figure 11(c)). The first step of ca. 10% from 50 to 350 °C could be attributed to desorption of the water. Since the lose of water, formed from the condensation of silanols in the silica framework, the second significant weight loss of ca. 80% between 350 and 460 °C was assigned to the decomposition of P123 and PVP. Nitrogen adsorption-desorption isotherms were measured on an ASAP 2010 volumetric adsorption apparatus (Micrometrics) at 77.4 K (Figure 11(d)). The surface area was calculated by using the BET method. The pore size distribution was calculated based on BJH method. It was found that the N_2 adsorption–desorption isotherm of the silica nanofiber is classified as typically

type-IV according to IUPAC nomenclature.[20] Also, an average fiber diameter, average pore diameter, and surface area of synthesized silica fiber were about 300 nm, 2.7 nm and 607 $m^2 g^{-1}$.

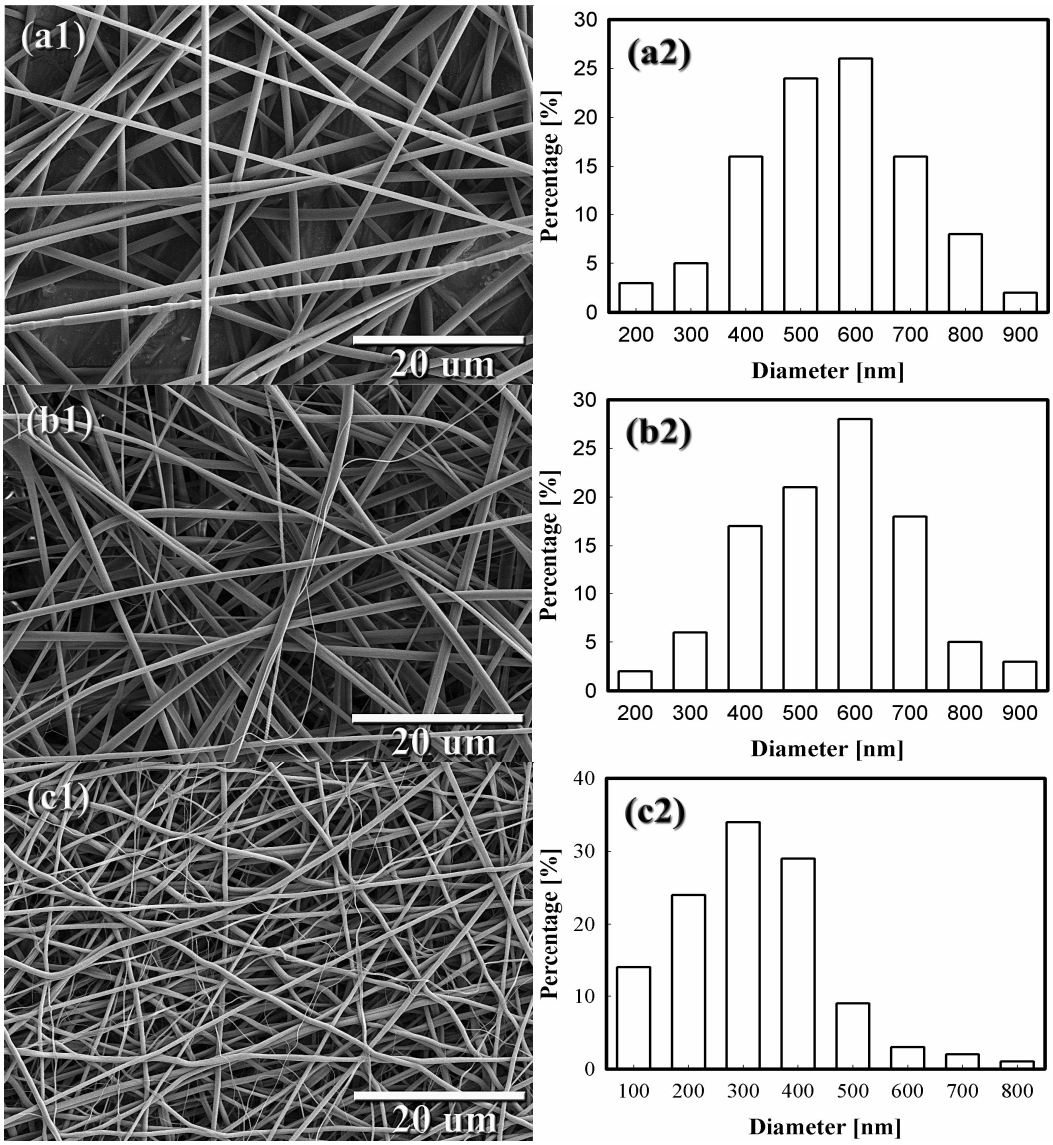

Figure 10. SEM images of the PVP fibers (a1), the as-electrospun silica/PVP fibers (b1), the silica nanofibers (c1), and the distribution of the diameter of the nanofibers (a2, b2, c2).

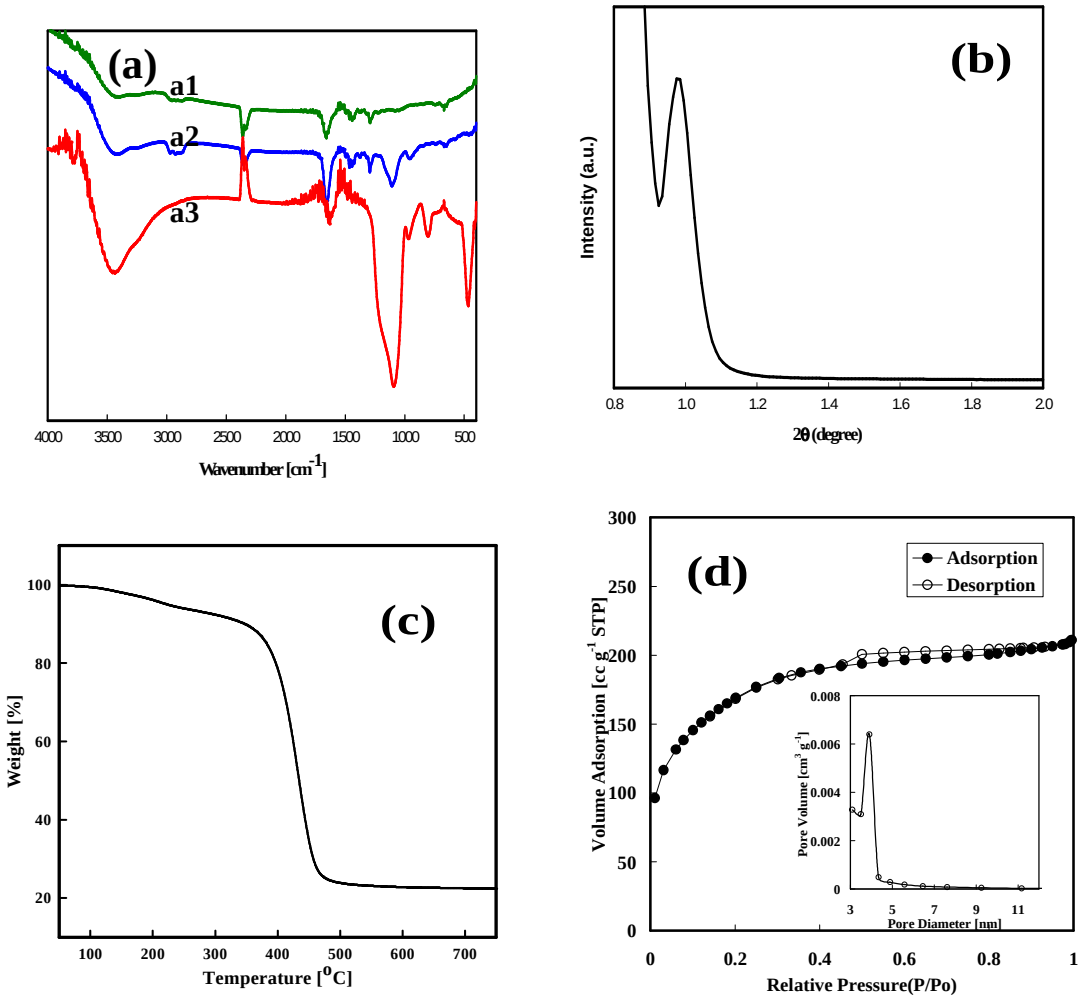

Figure 11. Characterization of various samples: (a) FT-IR spectra of the PVP fibers (a1), the as-electrospun silica/PVP fibers (a2) and the silica nanofibers (a3), (b) XRD pattern of silica nanofibers, (c) TGA curve of silica nanofiber, and (d) nitrogen adsorption-desorption isotherm and the calculated pore size of the silica nanofibers (inset).

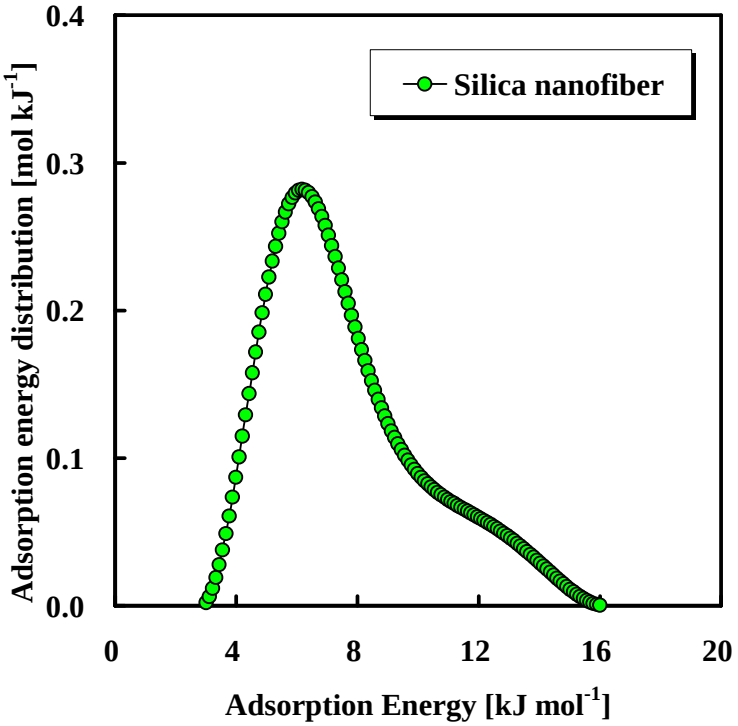

Figure 12. Adsorption energy distribution curve of the silica nanofiber.

On the other hand, adsorption energy distributions have been extensively applied in characterizing the numerous adsorption systems and in understanding the physico-chemical networks related to surface energy heterogeneities. Experimental adsorption isotherm data have been crucial factors for characterizing the surface energy heterogeneity of adsorbent.[7] Also, a theoretical local adsorption isotherm equation and an adsorption energy distribution function should be included. The overall adsorption isotherm on the heterogeneous solid surface can be written in the form of

$$\theta_T(p) = \int_\Delta \theta_L(p,U) \cdot F(U) dU \tag{4}$$

where p is the equilibrium pressure, Δ is the integration region, $\boldsymbol{U}$ is the adsorption energy,

F(U) is the wanted energy distribution function, $\theta_L(p,U)$ is a local adsorption isotherm and $\theta_T(p)$ is the experimental adsorption isotherm data. In this work, we employed the generalized regularization method to obtain reliable and stable adsorption energy distributions.[8] The adsorption energy distribution of silica nanofiber is presented in Figure 11 (d). The highest adsorption energy peaks was found to be around 6 kJ mol^{-1}. It can be seen from this result that silica nanofiber synthesized in this work is an energetically and structurally heterogeneous surface. Based on the characterization results, it is clear that the electrospinning is potentially a feasible method to obtain nanofibers using different templates.

To evaluate the adsorption properties of the synthesized nanofibers, adsorption isotherm of lysozyme as a model protein was investigated. It has been known that the molecular weight and isoelctric point of lysozyme have been 14,400 and pH=11.[21] Figure 12 shows the adsorption isotherm of lysozyme on silica nanofiber at pH 11 and 298.15 K. The solid lines in Figure 12 are the predicted results with Langmuir isotherm:

$$q = \frac{q_m bC}{1+bC} \tag{5}$$

Here, the physical meaning of isotherm parameters of q_m and b is the monolayer adsorption quantity and adsorbate-adsorbent affinity, respectively. The isotherm parameters (q_m and b) were determined by minimizing the mean percentage deviations between experimental and predicted amounts adsorbed on the basis of a modified Levenberg-Marquardt method (IMSL routine DUNSLF).[22] The object function, *E(%)*, represents the average percent deviation between experimental and predicted results as follows:

$$E(\%) = \frac{100}{n}\sum_{k=1}^{n}\left[\frac{\left|q_{\exp,k} - q_{cal,k}\right|}{q_{\exp,k}}\right] \tag{6}$$

where n is the number of experimental data, $q_{exp,k}$ is the experimental adsorption capacity, and $q_{cal,k}$ is the calculated adsorption capacity. The determined isotherm parameters of lysozyme on silica nanofiber are listed in Table 6. It is noted that the adsorption capacity of lysozyme was considerably high. The high capacity is attributed to two factors: the very high specific surface area available in the silica nanofibers, and the minimization of repulsive electrostatic interactions between adsorbed protein as a result of adsorption close to the protein pI. The silica nanofibers synthesized in this work can be successfully used in the field of sensor, chromatographic packing material, adsorption, and catalysis.

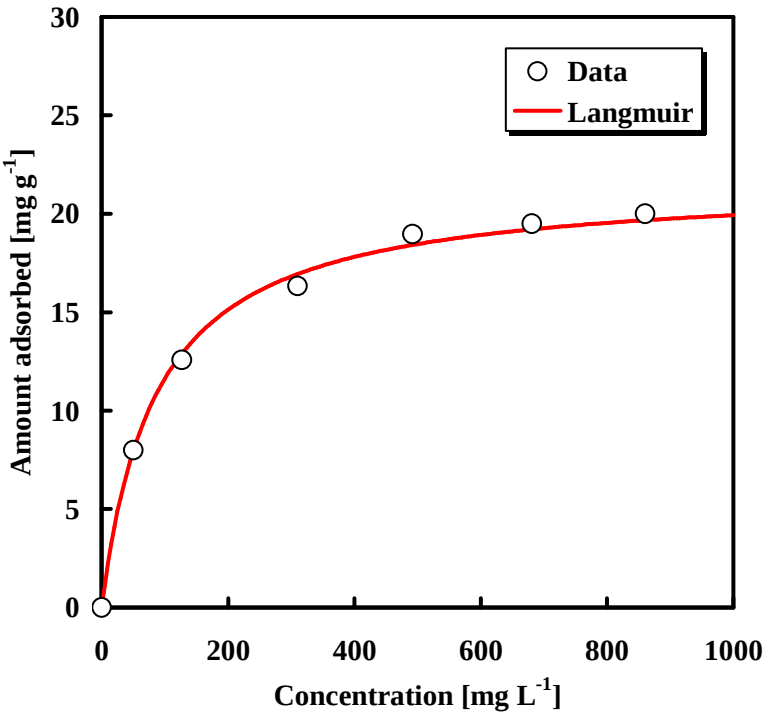

Figure 13. Adsorption isotherms of lysozyme on silica nanofibers at pH 11 and 298.15 K.

Table 6. Isotherm Parameters of Lysozyme

Isotherms	Parameters		E(%)
Langmuir	q_m	21.2	6.04
	b	0.011	

3.4. CONCLUSION

Silica nanofibers with smooth surface and high surface area were successfully synthesized by electrospinning method. Here, PVP and P123 were used as the fiber template and the structure directing agent. The synthesized samples were characterized by XRD, SEM, FT-IR, and BET. An average fiber diameter, average pore diameter, and surface area of the silica fibers are about 300 nm, 2.7 nm and 607 m^2 g^{-1}.The adsorption capacity of lysozyme on the synthesized silica nanofibers was high (i.e., 21.2 mg g^{-1}) because of the very high specific surface area available in the silica nanofibers, and the minimization of repulsive electrostatic interactions between adsorbed proteins. Also, adsorption equilibrium data were correlated well with the Langmuir and Sips equations. This study has proved that electrospinning is a potentially reliable method to obtain nanofibers using different templates. The silica nanofibers synthesized in this work may be widely used in the field of sensor, chromatographic packing material, catalysts, adsorbents and optical devices.

Chapter 4. Preparation and Characterization of Electrospun TiO_2 Nanofibers for Dye-Sensitized Solar Cell

4.1. Introduction

The electrochemical photovoltaics have been studied using wide-bandgap semiconductors, such as TiO_2, ZnO, Nb_2O_5, SnO_2, etc. [23-25]. In 1991, Gr¨atzel and co-worker [26] reported the dye-sensitized solar cell (DSSC) using nanocrystalline TiO_2 particles which increased the surface area several hundred times compared to those in compact semiconductor and electrolyte interfaces. The energy conversion efficiency of DSSC reaches over 10%, which is comparable to that of the silicon based solar cell [27]. In organic/inorganic hybrid solar cells, nanorods [28] and nanotubes [29] have been investigated as new electrode materials with a higher degree of order than the random assembly of nanoparticles. Recently, the electrospinning technique has been developed, which provides a simple, cost-effective approach for producing nanofibers within a broad range of diameters, from tens of nanometers to a few micrometers according to the selection of the processing parameters [30-32]. We demonstrated the porous electrode structure based on electrospun TiO_2 nanofibers, in which the energy conversion efficiency, the photocurrent generation with polymer gel electrolyte, was over 90% of the performance in DSSC with liquid electrolyte [33]. However, the volume content of TiO_2 in nanofiber web electrode is still low to maximize the photocurrent generation. In this study, the electrospun TiO_2 nanofibers are treated chemically to increase the TiO_2 volume content by using epitaxial growth of TiO_2 rutile crystal from aqueous $TiCl_4$ solution. The additional rutile layer modified the photocurrent generation of DSSC based on electrospun TiO_2 electrode. The energy conversion efficiency increases 30% after

post-treatment.

4.2 Experimental

TiO_2 fibers were electrospun directly onto a SnO_2:F-coated glass substrate (FTO, 1 cm×1 cm, TEC-8, Pilkingotn) from mixture containing 3 g poly(vinyl acetate) (PVAc,MW = 500,000 g/mol) (Aldrich), 6 g titanium(IV) isopropoxide (TiP) (Aldrich) and 2.4 g of acetic acid as a catalyst for sol-gel reaction in dimethyl formamide (DMF) (37.5 mL). In a typical electrospinning, the precursor solution was loaded into a syringe connected to a high-voltage power supply (ConverTech Model SHV120). An electric field of 15 kV was applied between a metal orifice and the FTO substrate at a distance of 10 cm. The spinning rate was controlled by a syringe pump (KD Scientific Model 220) at 60 L/min. Electrospun TiO_2 web was treated with tetrahydrofuran (THF) vapor in a closed chamber for 1 h prior to calcination. The calcination was carried out stepwise at each temperature (duration in min) as: 100 .C (15); 150 .C (15); 325 .C (5); 450 .C (30 min) in air. To grow TiO_2 rutile crystal epitaxially, TiO_2 web plate was immersed into a 0.1M titanium tetrachloride ($TiCl_4$) (Aldrich) aqueous solution in a closed chamber for 24 h. The 0.1M $TiCl_4$ aqueous solution was prepared in the following manner. At first, 2M concentrated $TiCl_4$ solution was prepared by adding directly titanium tetrachloride into a flask containing ice and then, the solution was further diluted to 0.1 M. The TiO_2 web electrode was immersed overnight in an ethanolic solution containing 3×10.4 M of ruthenium dye, $RuL_2(NCS)_2$ (L = 2,2-bipyridyl-4,4-dicarboxylic acid) (N3, Solaronix). The electrode was rinsed and dried after its removal from the dye solution. The liquid electrolyte we used consisted of 0.6M1-hexyl-2,3-dimethyl-imidazolium iodide (C6DMIm), 0.05M iodine (I_2), 0.1M lithium iodide (LiI) and 0.5M 4-tertbutylpyridine dissolved in 3-methoxyacetonitrile. Pt-sputtered SnO_2:F glass was used as the counter electrode.

The typical active area of DSSC was 0.25 cm^2. The photocurrent-voltage characteristics were measured with Keithley 2400 SMU under the global AM1.5, 100 mW/cm^2 irradiation. The incident photonto-current conversion efficiency (IPCE) was measured using a 350W Xe lamp light source with a motorized monochromator. Incident light intensity was calibrated using a Newport 818UV photodiode detector. The electrochemical impedance spectra (EIS) were obtained by Solatron FRA 1260 with EG&G PARC Potentiostat/Galvanostat Model 273 with an ac amplitude of 10mV at the open-circuit voltage (Voc) under illumination.

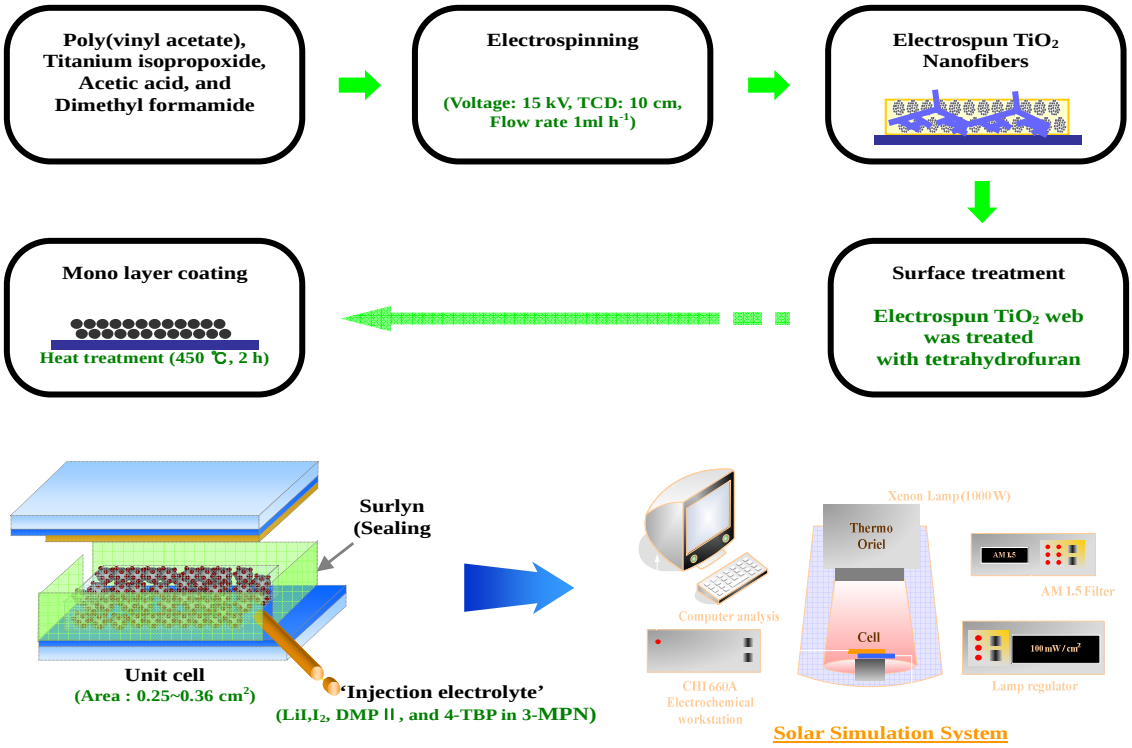

Figure 14. Procedure of TiO_2 fibers synthesis and photoelectrode fabrication.

4.3. Results and Discussion

Nanoporous electrospun TiO_2 electrodes improve the penetration of polymer gel electrolyte effectively. Electrospun TiO_2 web for DSSC in this work shows the well-organized porous electrode structure as shown in Figure 15 after calcination at 450 ℃ in air removing PVAc from the as-spun fibers. Several studies have previously reported that treatment of nanocrystalline TiO_2 with $TiCl_4$ solution. The result is a significant improvement in device performance.[34] The nanocrystalline TiO_2 electrode with $TiCl_4$ treatment increased the necking between the nanoparticles of the film, thus, facilitating the diffusion of photoinjected electron between particles and lowering the probability of recombination. In this study, electrospun TiO_2 web was treated with 0.1M $TiCl_4$ aqueous solution at different temperatures. The TiO_2 crystal grown from $TiCl_4$ is known by the rutile structure. The base TiO_2 web is anatase as shown Figure 17 and the epitaxially grown rutile is confirmed from the mixture of anatase and rutile peaks in Figure 17 after treatment. The epitaxial growth rate of rutile crystal on the anatase TiO_2 nanofiber surface depends on temperatures. After treatment at 20 ℃ for 24 h, TiO_2 fibers were covered with a small amount of rutile crystal as shown in Figure 15. The TGA curve of the as-electrospun TiO_2/PVAc fibers showed two steps and a total loss of ca. 70% (figure 16). The first step of ca. 60% from 50 to 350 could be attributed to desorption of the water and decomposition of PVAc. The second significant weight loss of ca. 10% from 350 to 500 was assigned to change TiO_2 crystallication anatase to rutile.

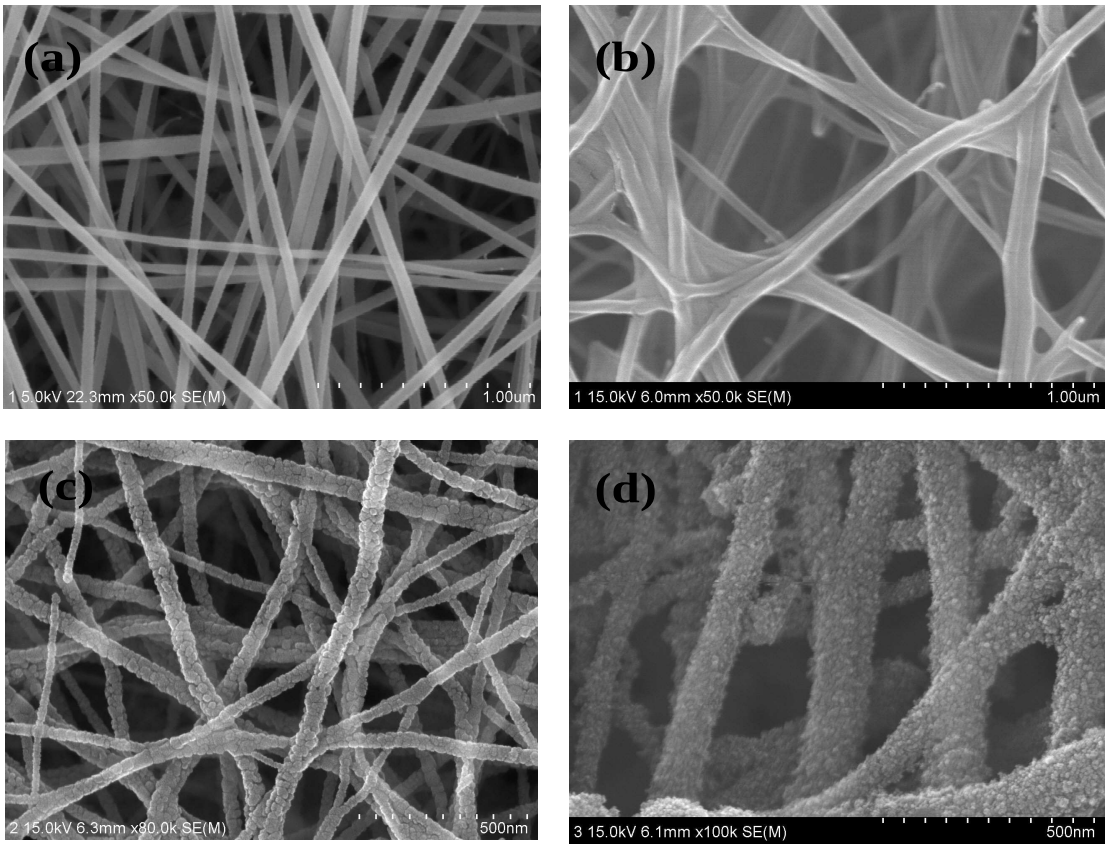

Figure 15. SEM images of electrospun TiO_2 nanofiber electrodes.(a) as-electrospun TiO_2 fiber; (b) After treated with tetrahydrofuran (THF) vapor in a closed chamber for 1h; (c) TiO_2 nanofiber; (d) After $TiCl_4$ aqueous solution treatment for 24h.

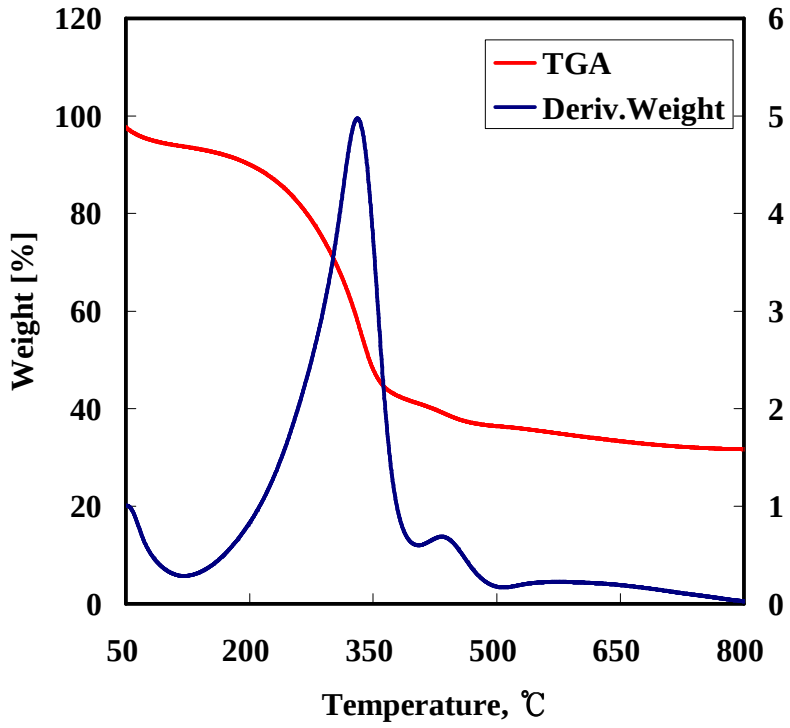

Figure 16. TGA curve of as-electrospun TiO_2 fibers.

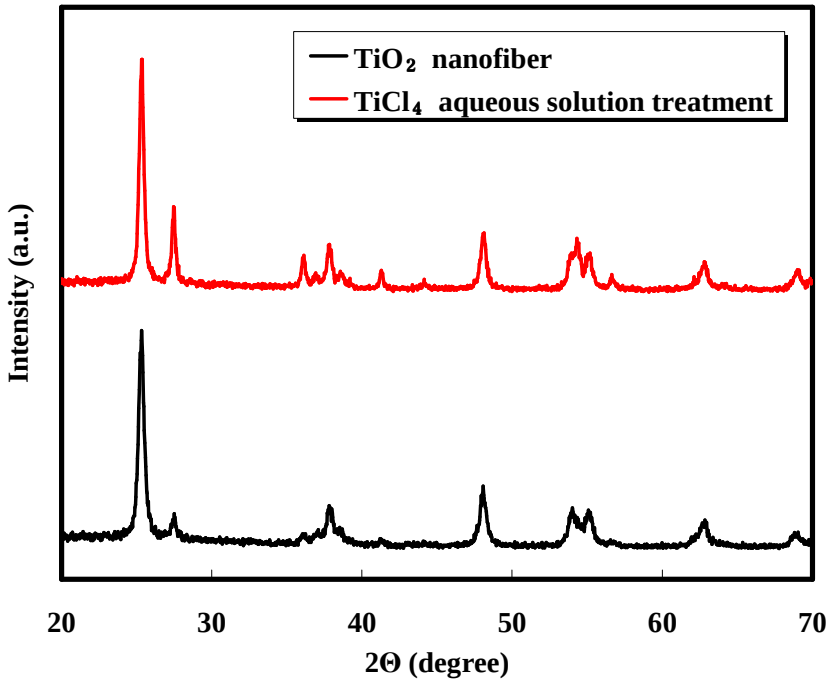

Figure 17. XRD pattern of TiO_2 fibers.

At 40 ℃, the diameter of TiO_2 fiber increased twice compared to the untreated $TiCl_4$ aqueous solution treatment as shown in Figure 14 and also the macroscopic porous morphology was retained. However, the treatment at higher temperature, such as 60 ℃ increases the additional rutile on the nanofibers and the porosity decreases to prevent the penetration of gel electrolyte.

Figure 18 presents the photocurrent density-voltage curves for cells based on electrospun TiO_2 nanopaticle, TiO_2 nanofiber and $TiCl_4$ treated TiO_2 nanofiber. The photovoltaic characteristics of DSSC based on TiO_2 nanopaticle, TiO_2 nanofiber and $TiCl_4$ treated TiO_2 nanofiber is seen in Table 7.

The open-circuit voltage (Voc) is relatively higher than that of typical nanocrystalline DSSCs. The $TiCl_4$ treatment of the electrode at 40 ℃ resulted in an increase in short-circuit photocurrent

(Jsc) increases from 8.67 to 11.24 mA/cm^2 for the liquid electrolyte device and in an increase in energy conversion efficiency (η) from 4.01 to 5.02 % (Figure 18).

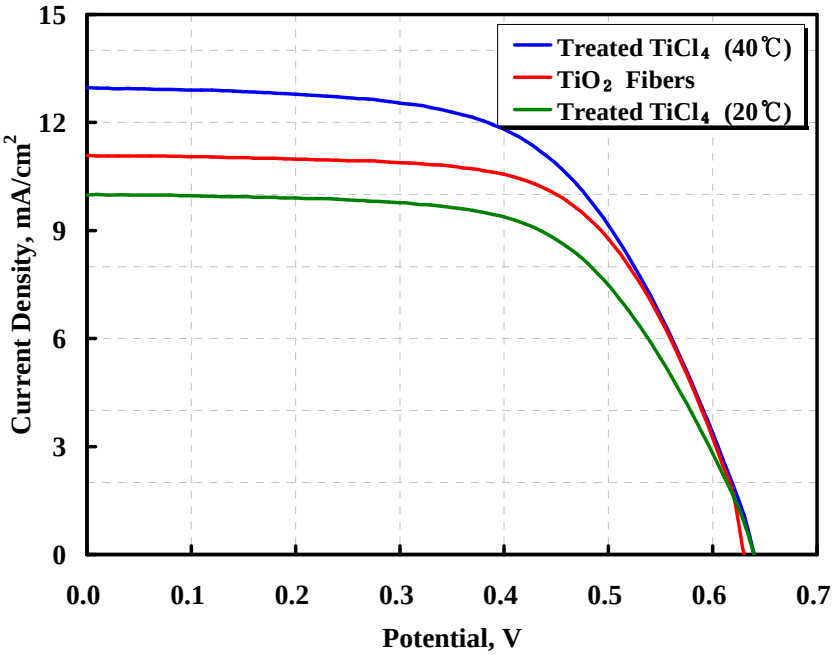

Figure 18. I-V Curve of DSSC.

Table 7. Photovoltaic performance of dye-sensitized solar cells

	Voc [V]	Isc(mA/cm2)	FF	η[%]
TiO_2 nanofiber	0.63	11.08	0.65	4.52
TiO_2 nanofiber - $TiCl_4$ treatment (20℃)	0.64	10.00	0.62	3.94
TiO_2 nanofiber - $TiCl_4$ treatment (40℃)	0.64	12.97	0.59	4.88

4.4. CONCLUSION

In summary, we obtained TiO_2 nanofibers diameter in the range of 80~100 nm. In order to improve the short-circuit photocurrent, we treated the electrospun TiO_2 electrode with $TiCl_4$ aqueous solution. The rutile crystalline layer was grown epitaxially on TiO_2 fibers. An additional TiO_2 layer increased the volume fraction of active materials in porous electrode resulting in an increase of sensitizer adsorption. The photocurrent of the DSSC with the electrospun TiO_2 electrode increased more than 10% after $TiCl_4$ treatment.

References

1. Hayati, I; Bailey, A.I; Tadros, T.F., *J Colloid Interface Sci.*, 117, 205 **(1987)**.
2. Taylor, G.I., Proc. Roy. *Soc. London*, A313, 454 **(1969)**.
3. Doshi, J & Reneker, D.H., *J. of Electrostat.*, 35, 151 **(1995)**.
4. C. Kim and K.S. Yang, *Applied physics letters*, 83, 1216 **(2003)**.
5. S.H. Park, C. Kim, Y.O. Choi, K.S.Yang, *Carbon*, 41, 2655 **(2003)**.
6. C. Kim, Y.J. Kim, Y.A. Kim, *Solid State Comm.*, 132, 567-571 **(2004)**.
7. M. Jaroniec and R. Madey, Physical Adsorption on Heterogeneous Solids, Elsevier, Amsterdam **(1988)**.
8. W. Rudzinski and D. Evertt, Adsorption of Gases on Heterogeneous Solids Surfaces, Academic Press, London **(1991)**.
9. J. S. Beck, J. C. Vartuli, W. J. Roth, M. E. Leonowicz, C. T. Kresge, K. D. Schmitt, C. T. Chu, D. H. Olson and E. W. Sheppard, *J. Am. Chem. Soc*. 114, 10834 **(1992)**.
10. J. Boucle, A. Kassiba, J. Emery, I. V. Kityk,M.Makowska-Janusik, J. Sanetra, N. Herlin-Boime and M. Mayne, *Phys. Lett. A.* 302, 196 **(2002)**.
11. J. W. Lee, W. G. Shim, H. Moon, *Microporous and Mesoporous Mat.* 73, 109 **(2004)**.
12. W. G. Shim, J. W. Lee, H. Moon, *Microporous and Mesoporous Mat.* 88, 112 **(2006)**.
13. W. G. Shim, H. Moon, J. W. Lee, *Microporous and Mesoporous Mat.* 94, 15 **(2006)**.
14. F. Marlow, B. Spliethoff, B. Tesche, D. Zhao, *Adv. Mater.* 12, 961 **(2000)**.
15. D. Li and Y.N. Xia, *Adv. Mater.* 16, 1151 **(2004)**.
16. H. Y. Wang, X. F. Lu, Y. Y. Zhao and C. Wang, *Mater. Lett.* 60, 1480 **(2006)**.
17. A. Corma, *Chem. Rev*. 97, 2373 **(1997)**.
18. Q. Zhao, Z. Huang, C. Wang, Q. Zhao, H. Sun and D. Wang, *Materials Letters* 61, 2159

(2007).

19. J.W. Lee, H.C. Kang, W.G. Shim, C. Kim, K.S. Yang, H. Moon, *J. Nanoscience and Nanotechnology* 6, 3577 **(2006)**.
20. F. Rouquerol, J. Rouquerol, K. Sing, Adsorption by Powders and Porous Solids, Academic Press: London, **(1999)**.
21. A. Katiyar, L. Ji, P. Smirniotis and N. G. Pinto, *J. Chromatography A* 1069, 119 **(2005)**.
22. J. B. Riggs, An Introduction to Numerical Methods for Chemical Engineers, Texas Tech. Uni. Press: Lubbock, **(1988)**.
23. A. Hagfeldt, M. Gratzel, *Chem. Rev.* 95, 49 **(1995)**.
24. K. Hara, T. Horiguchi, T. Kinoshita, K. Sayama, H. Sugihara, H. Arakawa, *Sol. Evergy Mater. Sol. Cells* 64, 115 **(2000)**.
25. K. Keis, C. Bauer, G. Boschloo, A. Hagfeldt, K. Westermark, H. Rensmo, H. Siegbahn, *J. Photochem. Photobiol. A Chem*. 148, 57 **(2002)**.
26. B. O'Regan, M. Gratzel, *Nature* 353, 737 **(1991)**.
27. M. Gratzel, *Nature* 414, 338 **(2001)**.
28. W.U. Huynh, J.J. Dittmer, A.P. Alivisatos, *Science* 295, 2425 **(2002)**.
29. M. Adachi, Y. Murata, I. Okada, S. Yoshikawa, *J. Electroshem. Soc*. 150, G488 **(2003)**.
30. D. Li, Y. Xia, *Nano Lett.* 3, 555 **(2003)**.
31. Z.-M. Hung, Y.-Z. Zhang, M. Kotaki, S. Ramakrichna, *Compos. Sci. Technol.* 63, 2223 **(2003)**.
32. A. Frenot, I.S. Chronakis, *Curr. Opin. Colloid Interface Sci*. 8, 64 **(2003)**.
33. M.Y. Song, D.K. Kim, K.J. Ihn, S.M. Jo, D.Y. Kim, ICSM2004 Proceedings, EMCS24V.
34. C.J. Barbe, F. Arendse, P. Comte, M. Jirousek, F. Lenzmann, V. Shklover, M. Gratzel, *J. Am.*

Ceram. Soc. 80, 3157 **(1997)**.

저작물 이용 허락서

학 과	화학공학과	학 번	20077091	과 정	석사
성 명	한글:이 윤 아 한문 : 李 允 雅 영문 : Lee Yoon Ah				
주 소	광주광역시 동구 지산 2 동 452-10 동산빌라 303 호				
연락처	E-MAIL : bungbung42@nate.com				
논문제목	한글 : 전기방사를 이용한 나노섬유 제조 및 특성 연구 영어 : Fabrication and Characterization of Nanofibers by Electrospinning				

본인이 저작한 위의 저작물에 대하여 다음과 같은 조건아래 -조선대학교가 저작물을 이용할 수 있도록 허락하고 동의합니다.

- 다 음 -

1. 저작물의 DB 구축 및 인터넷을 포함한 정보통신망에의 공개를 위한 저작물의 복제, 기억장치에의 저장, 전송 등을 허락함
2. 위의 목적을 위하여 필요한 범위 내에서의 편집·형식상의 변경을 허락함. 다만, 저작물의 내용변경은 금지함.
3. 배포·전송된 저작물의 영리적 목적을 위한 복제, 저장, 전송 등은 금지함.
4. 저작물에 대한 이용기간은 5 년으로 하고, 기간종료 3 개월 이내에 별도의 의사 표시가 없을 경우에는 저작물의 이용기간을 계속 연장함.
5. 해당 저작물의 저작권을 타인에게 양도하거나 또는 출판을 허락을 하였을 경우에는 1 개월 이내에 대학에 이를 통보함.
6. 조선대학교는 저작물의 이용허락 이후 해당 저작물로 인하여 발생하는 타인에 의한 권리 침해에 대하여 일체의 법적 책임을 지지 않음
7. 소속대학의 협정기관에 저작물의 제공 및 인터넷 등 정보통신망을 이용한 저작물의 전송·출력을 허락함.

동의여부 : 동의( ) 반대(O)

2008 년 11 월 일

저작자 : 이 윤 아 (서명 또는 인)

조선대학교 총장 귀하